Phase coexistence and particle nonconservation in a closed asymmetric exclusion process with inhomogeneities

Tirthankar Banerjee,[1,*] Anjan Kumar Chandra,[1,2,†] and Abhik Basu[1,‡]
[1]*Condensed Matter Physics Division, Saha Institute of Nuclear Physics, Calcutta 700064, India*
[2]*Department of Physics, Malda College, Malda, India*
(Received 11 March 2015; published 13 August 2015)

We construct a one-dimensional totally asymmetric simple exclusion process (TASEP) on a ring with two segments having unequal hopping rates, coupled to particle nonconserving Langmuir kinetics (LK) characterized by equal attachment and detachment rates. In the steady state, in the limit of competing LK and TASEP, the model is always found in states of phase coexistence. We uncover a nonequilibrium phase transition between a three-phase and a two-phase coexistence in the faster segment, controlled by the underlying inhomogeneity configurations and LK. The model is always found to be half-filled on average in the steady state, regardless of the hopping rates and the attachment-detachment rate.

DOI: 10.1103/PhysRevE.92.022121 PACS number(s): 05.70.Ln, 05.60.Cd

I. INTRODUCTION

Totally asymmetric simple exclusion process (TASEP) and its variants with open boundaries in one dimension (1D) serve as simple models of restricted 1D transport. These 1D transports are observed in a variety of situations, e.g., motion in nuclear pore complex of cells [1], motion of molecular motors along microtubules [2], fluid flow in artificial crystalline zeolites [3], and protein synthesis by messenger RNA (mRNA) ribosome complex in cells [4]; see Refs. [5] for basic reviews on asymmetric exclusion processes. The coupled dynamics of TASEP and random attachment-detachment in the form of Langmuir kinetics (LK) displays a rich behavior, including coexistence of low- and high-density regions of particles and a boundary condition independent phase, in the limit when LK competes with TASEP [6]. Open TASEPs with defects, both point and extended, have been studied; see, e.g., Refs. [7], which investigated the effects of the defects on the steady-state densities and currents. In addition, open TASEP with a single point defect along with LK has been considered in Ref. [8], which finds a variety of phases and phase coexistences as a result of the competition between the defect and LK.

In recent studies involving asymmetric exclusion processes on closed inhomogeneous rings, the total particle number is held fixed by the dynamics, as expected in exclusion processes; see, e.g., Refs. [9–11]. Nonconserving LK is expected to modify the steady-state densities of pure TASEP on a closed inhomogeneous ring. TASEP on a perfectly homogeneous ring yields uniform steady-state densities, due to the translational invariance of such a system. Evidently, introduction of the particle nonconserving LK should still yield uniform steady-state densities, again due to the translational invariance of the system, although the actual value of the uniform steady-state density should now depend upon LK. Nonuniform or inhomogeneous steady states are expected only with explicit breakdown of the translation invariance, e.g., by means of quench disorder in the hopping rates at different sites. Studies on this model should be useful in various contexts, ranging from vehicular and pedestrian traffic to ribosome translocations along mRNA, apart from theoretical interests. For example, consider pedestrian or vehicular movement along a circular track with bottlenecks and constrictions, where overtaking is prohibited and pedestrians or vehicles can either leave and join the circular track (say, through side roads) randomly [5], or, for instance, consider the motion of ribosomes along closed mRNA loops with defects where the ribosomes can attach or detach to the mRNA loop stochastically [12].

In this article, we introduce a disordered TASEP on a ring with LK, where the disorder is in the form of piecewise discontinuous hopping rates across the two segments of the ring. The unidirectional hopping of the particles across a slow segment yields reduced particle current. Evidently, this breaks the translational invariance. Hence, inhomogeneous steady-state densities cannot be ruled out. In addition, we allow random attachment-detachment of the particles or LK at every site of the ring. Thus, the interplay of the quenched disorder in the hopping rate with the consequent absence of translation invariance and LK should determine the steady states of the model. For simplicity we assume equal rates for attachment and detachments. Our model is well-suited to analyze a key question of significance, viz., whether the steady-state density profiles and the average particle numbers in the steady states can be controlled by the disorder and (or) the LK. Recent studies of nonequilibrium steady states in TASEP on a ring with quenched disordered hopping rates without any LK revealed macroscopically inhomogeneous steady-state densities in the form of a localized domain wall (LDW) for moderate average particle densities in the system; see, e.g., Refs. [9,13]. Our work provides insight about how the steady states in the models in Refs. [9,13] are affected by particle nonconservation and allows us to study competition between bulk LK and asymmetric exclusion processes in ring geometry. To our knowledge, this has not been studied before. We generically find (i) nonuniform steady states and phase coexistences, (ii) phase transition between different states of phase coexistences, and (iii) the system is always half-filled in the steady state for the whole relevant parameter range, regardless of the detailed nature of the underlying steady-state

*tirthankar.banerjee@saha.ac.in
†anjan.chandra@saha.ac.in
‡abhik.basu@saha.ac.in

density profiles. The rest of the article is organized as follows. In Sec. II, we construct our model. Then we calculate the steady-state density profiles for an extended defect in Sec. III A and for a point defect in Sec. III B. In Sec. IV, we compare the results for extended and point defects. Next, in Sec. V, we discuss why the average density shows a fixed value for any choice of the phase parameters. Finally, in Sec. VI we summarize and conclude.

II. THE MODEL

We consider an exclusion process on a closed 1D inhomogeneous ring with N sites, together with nonconserving LK. The quenched inhomogeneity is introduced via space-dependent hopping rates. The parts with lower hopping rates can be viewed as defects in the system. Specifically, our model consists of two segments of generally unequal number of sites. We call the parts channel I (CHI), with N_1 sites (sites $i = 1,2,\ldots,M$) and unit hopping rate, and channel II (CHII), with N_2 sites (sites $i = M+1, M+2, \ldots, N$) and hopping rate $p < 1$, where $M < N$ (see Fig. 1). We consider both the cases of an extended and a point defect separately. The size of an extended defect scales with the system size, such that even in the thermodynamic limit, it covers a finite fraction of the ring (i.e., finite N_2/N in the limit $N \to \infty$). In contrast, the size of a point defect does not scale with the system size, and hence, the size of a point defect relative to the system size vanishes in the thermodynamic limit (i.e., $N_2/N \to 0$ for $N \to \infty$). Now consider an asymmetric exclusion process on the ring: A particle can hop in the anticlockwise direction to its neighboring site if and only if the site is empty. No two particles can occupy the same site and neither can a particle move backward even if there is a vacancy. Between CHI and CHII, particle exchanges are defined at the junctions A and B only (see Fig. 1), where dynamic rules are defined by the originating site. In addition, the system executes LK, e.g., at any site, a particle can either attach to a vacant site from the surroundings or leave an occupied site at a rate ω.

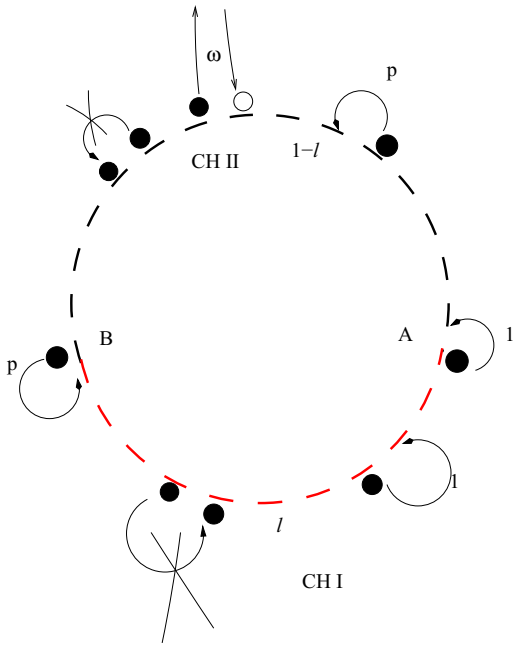

FIG. 1. (Color online) Particles hop with rates 1 and $p < 1$ in segments CHI (red) and CHII, respectively. $\omega = \Omega/N$ (see text) denotes both the evaporation and condensation rates; A and B are the junctions where the two segments meet.

With n_{Ii} and n_{IIi} as the steady-state number densities at ith sites of CHI and CHII, respectively, and $N_{\rm tot}$ the total number of particles in the system ($N_1 = lN, N_2 = (1-l)N$, l refers to the fraction of sites having hopping rate unity),

$$[n_I l + n_{II}(1-l)]N = N_{\rm tot}, \tag{1}$$

where $n_I = \sum_i n_{Ii}$, $n_{II} = \sum_i n_{IIi}$. Now define the mean-number density for the total system n as

$$n = \frac{N_{\rm tot}}{N} = n_I l + n_{II}(1-l). \tag{2}$$

Due to LK, n is not a conserved quantity and cannot be used to characterize the steady states in the model, unlike Ref. [9]. Rather, l, p, and ω parametrize the steady density profiles. In order to ensure that the total flux of the particles due to LK is comparable to the particle current due to the hopping dynamics of TASEP (i.e., the total detachment-attachment events of the particles due to LK should be comparable to the number of crossings of the junctions A and B by the particles in a given time interval), we introduce a scaling for the evaporation and condensation rates and define the total rate $\Omega = \omega N$ and analyze the system for a given $\Omega \sim O(1)$. This ensures competition between LK and TASEP; see, e.g., Ref. [6]. Although there is no particle number conservation either in Ref. [6] or here, it is important to emphasize one important difference between the two that stems from the fact that our model is closed. As a result, there is no injection or extraction of particles at designated "entry" or "exit" sites, unlike in open TASEP or the model in Ref. [6], where these rates are the tuning parameters.

III. STEADY-STATE DENSITIES

We perform mean-field (MF) analysis of our model, supplemented by its extensive Monte Carlo simulations (MCS).

A. MF analysis and MCS results for an extended defect

Before we discuss the details of the MF analysis of our model, it is useful to recall the results from the model in Ref. [6], where the steady-state densities of a TASEP with open boundaries together with LK having equal attachment and detachment rates, Ω are investigated. Depending upon the entry (α) and exit (β) rates and Ω, the steady-state densities can be low or high densities, or phase coexistences involving three or two phases. By varying the above control parameters, transitions between the different steady states are observed. Motivated by these results and considering the junctions between the two segments as the effective entry and exit points of the segments, it is reasonable to expect similar behavior including phase coexistences and transitions between them in our model. Our detailed analysis as given below partly validate these expectations; we show that our model displays phase coexistences, but has no analogs of the low- and high-density phases. We find that even in the case of a point defect where there is effectively only one junction, these remain true.

Our MF analysis is based on treating the model as a combination of two TASEPs—CHI and CHII, joined at the junctions A and B, respectively. Thus, junctions B and A are *effective* entry and exit ends of CHI. This consideration allows us to analyze the phases of the system in terms of the known phases of the open boundary LK-TASEP [6]. For convenience, we label the sites by a continuous variable x in the thermodynamic limit, defined by $x = i/N$, $0 < x < 1$. In terms of the rescaled coordinate x, the lengths of CHI and CHII are l and $1-l$, respectively. For an extended defect here, $l < 1$. Without the LK dynamics, the steady-state densities of a TASEP on an inhomogeneous ring may be obtained by means of the conservation of the total particle number and the particle current in the system [9–11]. In contrast, it is important to note that in the present model, due to the nonconserving LK dynamics, the particle current is conserved only *locally*, since the probability of attachment or detachment at a particular site vanishes as $1/N$ [6]. Similar to Ref. [6], the steady-state densities, $n_I(x)$, $n_{II}(x)$, follow

$$(2n_I - 1)\left(\frac{dn_I}{dx} - \Omega\right) = 0, \tag{3}$$

$$(2n_{II} - 1)\left(\frac{dn_{II}}{dx} - \Omega\right) = 0. \tag{4}$$

These yield $n_I, n_{II} = 1/2$ and $n_I, n_{II} = \Omega x + C_I/C_{II}$, where C_I,C_{II} are the integration constants.

Apply now the current conservation locally at A and B. Ignoring possible boundary layers, this yields

$$n_I(1 - n_I) = p n_{II}(1 - n_{II}) \tag{5}$$

separately, very close to $x = 0$ and $x = l$. Since $p < 1$ necessarily, Eq. (5) yields $n_I \neq 1/2$. Thus, either $n_I > n_{II}$ or $n_I < n_{II}$ very close to the junctions A and B. It is known that with $\Omega = 0$, $n_{II} = 1/2$ is a solution for moderate n, with $n_I(x)$ being in the form of a localized domain wall (LDW) [9,11]. Finite Ω is expected to modify these solutions. Nonetheless, since $n_{II} = 1/2$ is a solution of the steady-state Eq. (4), $n_{II} = 1/2$ remains a valid steady-state solution for nonzero Ω. Whether or not there are other solutions for n_{II} is discussed later. With $n_{II} = 1/2$, we obtain $n_I(x)$ at $x = 0,l$ by Eq. (5).

Application of Eq. (5) yields

$$n_I = \frac{1 \pm \sqrt{1-p}}{2}, \tag{6}$$

at $x = 0,l$, which serve as boundary conditions on $n_I(x)$. It is useful to compare CHI with an open TASEP. We identify effective entry (α_e) and exit (β_e) rates: $\alpha_e = \beta_e = (1 - \sqrt{1-p})/2 \leqslant 1/2$. Considering the fact that the hopping rate p of CHII is less than that in CHI (unit value), on physical grounds, we expect particles to accumulate behind junction A in CHI only. In other words, we expect $n_I(x = l) \geqslant n_I(x = 0)$. These considerations allow us to set the boundary conditions $n_I(x = 0) = [1 - \sqrt{1-p}]/2$ and $n_I(x = l) = [1 + \sqrt{1-p}]/2$. Hence, from Eq. (3) we arrive at the three following solutions for $n_I(x)$, namely

$$n_{I\alpha}(x) = \Omega x + \frac{1 - \sqrt{1-p}}{2}, \tag{7}$$

$$n_{I\beta}(x) = \Omega(x - l) + \frac{1 + \sqrt{1-p}}{2}, \tag{8}$$

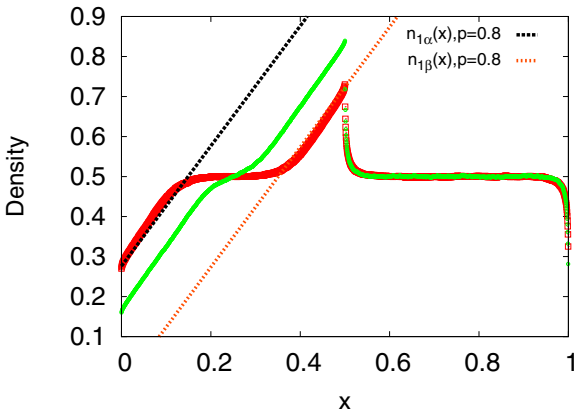

FIG. 2. (Color online) Steady-state density profiles showing three-phase coexistence in CHI for $l = 0.5$, $N = 2000$. The left and right solutions meet at $n(x) = 1/2$ in the bulk. Square points represent MCS results for $p = 0.8, \Omega = 1.5$; while the deep and shaded lines show the corresponding MFT equations for $n_{1\alpha}$ and $n_{1\beta}$. The circular points represent MCS studies for $p = 0.55, \Omega = 1.5$. Clearly, the length of the MC region varies depending on the parameters, p and Ω.

and

$$n_{Ib} = \tfrac{1}{2}, \tag{9}$$

where $n_{I\alpha}(x)$ and $n_{I\beta}(x)$ are the linear density profiles satisfying the boundary conditions at the entrance (B) and exit (A) ends of CHI and n_{Ib} represents the MC region. Notice that the solution $n_{Ib} = 1/2$ cannot be extended to the junctions A and B, else Eq. (5) will be violated.

Given the physical expectation that $n_I(x)$ should not decrease with x, we identify two values of x, viz., x_α and x_β, where the linear solutions meet with the third solution. Depending on these values of x_α and x_β, we will see that the system is found in various phases, which are parametrized by p and Ω. Using $n_{I\alpha}(x_\alpha) = n_{I\beta}(x_\beta) = \frac{1}{2}$, we get $x_\alpha = \frac{\sqrt{1-p}}{2\Omega}$ and $x_\beta = l - \frac{\sqrt{1-p}}{2\Omega} = l - x_\alpha$. Thus, we find

$$x_\beta - x_\alpha = l - \frac{\sqrt{1-p}}{\Omega}. \tag{10}$$

Hence, there are three distinct possibilities, namely $x_\alpha = x_\beta$, $x_\alpha < x_\beta$, and $x_\alpha > x_\beta$, depending on which the system will be found in different phases. We now analyze each of the cases in detail.

(1) Consider $x_\alpha < x_\beta$. Here we observe a three-phase coexistence. Near $x = 0$, we see a low-density (LD) phase having density $n_{Ix} < 1/2$, rising with a positive slope up to $x = x_\alpha$. For $x_\alpha < x < x_\beta$, there is a maximal current (MC) phase with $n_{Ix} = 1/2$ and the current $J_{Ix} = 1/4$, and while $x_\beta < x < l$, we see a high-density (HD) phase with $n_{Ix} > 1/2$. This is accompanied by an MC phase in CHII. Representative plot of comparisons of MFT and MC results are shown in Fig. 2.

(2) When $x_\alpha = x_\beta$, the maximal current region separating the two linear solutions vanishes and the density profile becomes an inclined straight line, matching continuously the densities of the LD and HD phases; see Fig. 3.

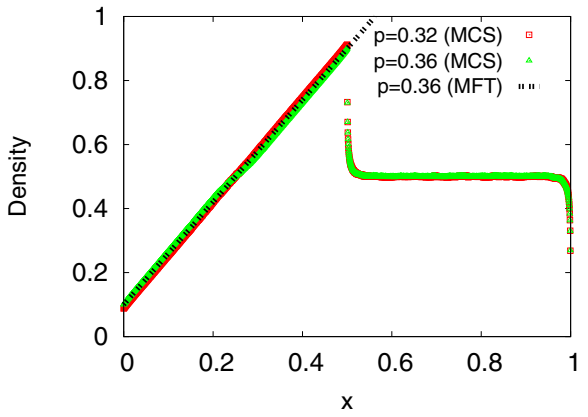

FIG. 3. (Color online) Straight-line density profile for the extended defect ($x_\alpha = x_\beta, l = 0.5, N = 2000$) in CHI. The dotted black line represents the MFT denisty profile equation for $\Omega = 1.6$, $p = 0.36$, and the triangular points shows the corresponding MCS result. The square points correspond to the MCS density profile for $\Omega = 1.6$, $p = 0.32$.

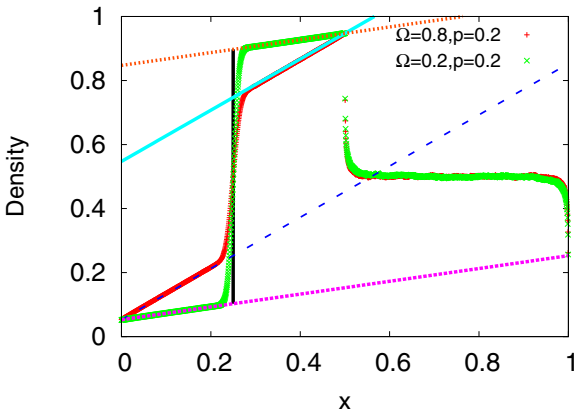

FIG. 4. (Color online) Formation of an LDW in CHI for $x_\alpha > x_\beta$ with $l = 0.5$, $N = 2000$. Two different data sets have been plotted for p and Ω. Points represent MCS results. The lines represent the following (all MFT equations): broken rectangles ($n_{1\beta}$, $\Omega = 0.2$, $p = 0.2$), broken square ($n_{1\alpha}$, $\Omega = 0.2$, $p = 0.2$), solid ($n_{1\beta}$, $\Omega = 0.8$, $p = 0.2$), gapped ($n_{1\alpha}$, $\Omega = 0.8$, $p = 0.2$). As expected, the location of the domain wall remains fixed (continuous line at $x = 0.25$ represents the MFT DW).

(3) As $x_\alpha > x_\beta$, we can no more find the MC region and instead find a density discontinuity. Solutions from the left and right meet at a point x_w in the bulk of CHI in the form of a localized domain wall (LDW), where the left and right currents, i.e., $J_\alpha(x_w)$ and $J_\beta(x_w)$, are equal. We can arrive at an expression for x_w using the the local current conservations. Here, $J_\alpha(x_w) = n_{I\alpha}(x_w)[1 - n_{I\alpha}(x_w)]$. Similarly, $J_\beta(x_w) = n_{I\beta}(x_w)[1 - n_{I\beta}(x_w)]$. The equality of $J_\alpha(x_w)$ and $J_\beta(x_w)$ gives us the condition

$$n_{I\alpha}(x_w) + n_{I\beta}(x_w) = 1, \tag{11}$$

since $n_{I\alpha}(x_w) \neq n_{I\beta}(x_w)$. Using Eq. (11), $x_w = l/2$. Thus, the LDW is always at the midpoint of CHI, unlike in Refs. [10,11]. The fact that $x_w = l/2$ may be understood from the symmetrical structures of $n_{I\alpha}(x)$ and $n_{I\beta}(x)$. Notice that $1/2 - n_{I\alpha}(x = 0) = n_{I\beta}(x = l) - 1/2$. Since, the upward slope of $n_{I\alpha}(x)$ is same as the downward slope of $n_{I\beta}(x)$, which is Ω, equality of the currents $J_\alpha(x_w) = J_\beta(x_w)$ ensures that $x_w = l/2$. Thus, x_w is *independent of* the values of Ω and p. This is to be contrasted with Ref. [6], where Ω is known to affect the location of the LDW there. The height of the LDW is

$$\Delta h_e = n_{I\beta}(x_w) - n_{I\alpha}(x_w) = \sqrt{1 - p} - \Omega l, \tag{12}$$

which depends upon l, p, and Ω. In our MCS studies we have generally chosen $l = 1/2$ without any loss of generality. Since $l = 1/2$, the domain wall in CHI will always be located at $x_w = 1/4$, irrespective of the values of p and Ω. See Fig. 4 for a representative plot. The overall average density n may be found from (neglecting the boundary layers)

$$n = \int_0^l n_I(x)dx + \int_l^1 n_{II}(x)dx. \tag{13}$$

Substituting the MF forms of $n_I(x)$ and $n_{II}(x)$, it is clear that $n = 1/2$, regardless of whether CHI is in its two- or three-phase coexistence state. Our MCS results agree with the MF results to a good extent.

We now discuss why the system cannot be found in any other combination of the phases of an open TASEP. First of all, there is no possibility of only an MC phase in CHI. This follows from the fact that if $n_I = 1/2$, Eq. (5) would be violated at the boundaries. In order to have an LDW in CHII, particles should pile up behind CHI, which is physically unexpected since CHI has a higher hopping rate. Further, we argue that with an MC phase in CHII, CHI cannot be found in a pure LD phase. For CHI to be in such a phase, $x_\alpha = 1/2$. But it is also necessary that x_β has to be greater than x_α; otherwise, CHI will show an LDW. But the maximum possible value for x_β is $1/2$. Now, $x_\alpha = x_\beta = 1/2$ implies $p = 1$, for which the system becomes homogeneous. Since we necessarily have $p < 1$ in our model, a pure LD phase for CHI with an MC phase in CHII is ruled out. Due to the particle-hole symmetry, we rule out a pure HD phase for CHI with CHII in its MC phase. Last, both CHI and CHII cannot be in their LD phases. This may be understood as follows. The general solutions for Eqs. (3) and (4) are either inclined lines of the form $\Omega x + C_{I,II}$ ($C_{I,II}$ being constants) or flat ($1/2$). For LD phases, $C_{I,II}$ are to be determined by the density values at the entry sides of CHI and CHII, respectively. Let us assume $n_I(x = 0) = n_{Il}$ and $n_{II}(x = l) = n_{IIl}$. With these known values, $n_I(x = l)$ and $n_{II}(x = 1)$, respectively, in CHI and CHII can be determined. Say these values are n_{Ir} and n_{IIr} for the respective channels. Clearly, $n_{Ir} > n_{Il}$ and $n_{IIr} > n_{IIl}$. But n_{Ir} is connected to n_{IIl} at junction A by

$$n_{Ir}(1 - n_{Ir}) = p n_{IIl}(1 - n_{IIl}), \tag{14}$$

and n_{IIr} and n_{Il} are connected at junction B by

$$p n_{IIr}(1 - n_{IIr}) = n_{Il}(1 - n_{Il}). \tag{15}$$

Clearly, both Eqs. (14) and (15) cannot be satisfied, simultaneously. Hence, this rules out the LD-LD phase for the system. Similar arguments rule out simultaneous HD phases in both channels.

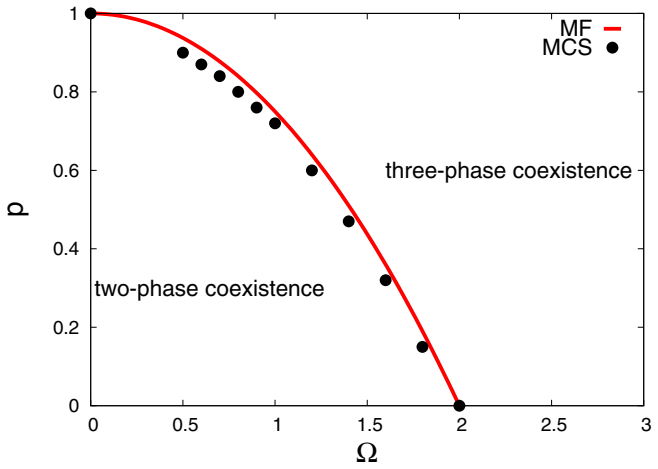

FIG. 5. (Color online) The phase diagram for $l = 0.5$. The curve $p = 1 - \frac{\Omega^2}{4}$ separates regions of two-phase and three-phase coexistences.

1. The phase diagram

We now discuss the phase diagram spanned in the Ω-p space. Consider the case when $x_\alpha = x_\beta$. Using Eq. (10),

$$\sqrt{1-p} = \Omega l, \tag{16}$$

which gives the phase boundary

$$p = 1 - [\Omega l]^2. \tag{17}$$

Thus, when $x_\alpha < x_\beta$, we have $p > 1 - [\Omega l_1]^2$ and the system shows three-phase coexistence of LD ($n_I < 1/2$), MC ($n_I = 1/2$), and HD ($n_I > 1/2$) regions in CHI. For $p < 1 - [\Omega l]^2$, we get an LDW in CHI. For both three-phase and two-phase coexistences in CHI, CHII will be in its MC phase. The phase diagram is shown in Fig. 5.

The width W of the MC region (numerically equal to $x_\beta - x_\alpha > 0$) in the three-phase coexistence, can be identified as the order parameter for the phase transition between a three-phase coexistence and a two-phase coexistence. When the system is in three-phase coexistence, $W > 0$, where as it is zero in the two-phase coexistence. For a fixed value of p, as Ω is increased, the system makes a transition from a two-phase coexistence state to a three-phase coexistence state following Eq. (17). Accordingly, W increases from 0 to l as Ω is increased for a fixed p. At the transition, $W = 0$. We now find how W approaches zero as $p \to p_c$ or $\Omega \to \Omega_c$ in the three-phase coexistence; p_c, Ω_c are located at the phase boundary given by Eq. (17). Writing $p = p_c + \delta p$, $\Omega = \Omega_c + \delta\Omega$ for small $\delta p > 0, \delta\Omega > 0$, we have

$$W = l - \frac{\sqrt{1-p_c}}{\Omega_c}[1 - \delta p/2 - \delta\Omega] = \frac{\sqrt{1-p_c}}{\Omega_c}(\delta p/2 + \delta\Omega), \tag{18}$$

to the linear order in $\delta p, \delta\Omega$. Evidently, W vanishes smoothly as δp and $\delta\Omega$, indicating the second-order nature of the phase transition. Thus, considering either p or Ω as the control parameter (for fixed Ω or p, respectively), and drawing analogy with equilibrium second-order phase transitions [14], we extract an "effective" order parameter exponent of value unity. This is to be contrasted with the MF order parameter exponent of value $1/2$ in equilibrium critical phenomena. This difference is not surprising, considering that the present model is inherently out of equilibrium.

B. Density profiles for a point defect

Consider now the extreme limit with $l \to 1$, i.e., with a point defect. In this limit, the system has only one site where the hopping rate p is less than 1, while for all other sites, the hopping rate is unity. Thus, the MF analysis above by considering the system to be a combination of two TASEP channels joined at two ends no longer works because CHII (as defined for an extended defect) now contains just one site and has a vanishing length relative to the whole system for $N \to \infty$. Instead, the system is just one TASEP, say CHI, with a density $n_I(x)$, $0 < x < 1$ and two of its ends joined at one site having a hopping rate $p < 1$.

Let the defect be present at $x = 0$ (which is same as $x = 1$). We assume that the particles are hopping anticlockwise as before. On physical grounds we expect piling up of particles (if at all) should occur behind the blockage site at $x = 0$.

Now assume a macroscopically nonuniform steady-state density profile, such that there is a pile up of particles behind the defect at $x = 0$ and hence a jump in the density at $x = 0$. Let ρ_I and ρ_{II} be the densities just to the left and right of $x = 0$, respectively: $n_I(1-\epsilon) = \rho_I, n_I(\epsilon) = \rho_{II}, \epsilon \to 0$. Using current conservation at $x = 0$, we write

$$\rho_I(1-\rho_I) = p\rho_I(1-\rho_{II}) = \rho_{II}(1-\rho_{II}). \tag{19}$$

This yields solutions for ρ_I and ρ_{II}, viz., $\rho_I = \frac{1}{1+p}$ and $\rho_{II} = \frac{p}{1+p}$. Density $n_I(x)$ satisfies the equation

$$(2n_I - 1)\left(\frac{dn_I}{dx} - \Omega\right) = 0, \tag{20}$$

yielding solutions

$$n_I(x) = 1/2, \Omega x + C. \tag{21}$$

The constant of integration C is to be fixed by using either of the boundary conditions ρ_I or ρ_{II}. These evidently yield two values of C, say C_R and C_L, respectively, giving $C_L = \frac{p}{1+p}$ and $C_R = \frac{1}{1+p} - \Omega$. Therefore, the two solutions of $n_I(x)$ are

$$\begin{aligned} n_L(x) &= \Omega x + \frac{p}{p+1}, \\ n_R(x) &= \Omega(x-1) + \frac{1}{p+1}, \end{aligned} \tag{22}$$

along with the uniform solution $n_b = 1/2$. Similar to an extended defect, we can compare CHI in case of point defect with an open TASEP and extract effective entry and exit rates: $\alpha_p = \beta_p = p/(p+1) < 1/2$, where α_p and β_p are entry and exit rates, respectively.

Since $n_L(x)$ and $n_R(x)$ depend linearly upon x, in general they should meet with the uniform solution, i.e., $n_b = 1/2$ at two points, say, x_L and x_R. The quantitative analysis follows the same logic as above for an extended defect. Accordingly, the values of x_L and x_R will determine whether the system is in its three-phase coexistence state or a two-phase coexistence

state. We find

$$x_L = \left(1/2 - \frac{p}{p+1}\right)\frac{1}{\Omega}, \tag{23}$$

$$x_R = \left(1/2 + \Omega - \frac{1}{1+p}\right)\frac{1}{\Omega}. \tag{24}$$

The system will thus be in three-phase coexistence when $x_L < x_R$ and we will have two inclined lines meeting the third solution in the bulk at x_L and x_R, respectively. The extent of the MC phase (bulk solution) is given by

$$x_R - x_L = 1 - \left(\frac{1-p}{1+p}\right)\Omega. \tag{25}$$

Similarly, for $x_L > x_R$, the system will be found in its two-phase coexistence state and the two inclined solutions will meet in the bulk in the form of an LDW. The location of the LDW, x_w^p may be calculated similarly as that for an extended defect, yielding $x_w^p = \frac{1}{2}$. The height of the LDW is density difference between $n_{IL}(x)$ and $n_{IR}(x)$ at $x = 1/2$, which is given by

$$\Delta h_p = n_R(x_p) - n_L(x_p) = \frac{1-p}{1+p} - \Omega. \tag{26}$$

Thus, with both an extended and a point defect, the location of the LDW is at the middle of CHI. Again, as for an extended defect, this is a consequence of the symmetry in the forms of $n_L(x)$ and $n_R(x)$. For $x_L = x_R$, the extent of the MC phase vanishes and one obtains a straight line smoothly connecting the densities n_L and n_R. Our MFT results here are complemented by extensive MCS studies. Plots of $n_I(x)$ versus x for various p and Ω in the steady states are shown in Figs. 6–8. As for an extended defect, we find the steady -state average density $n = 1/2$ in the steady state by using the MF form of $n_I(x)$ as given in Eq. (22), again in agreement with the corresponding MCS results. Last, there are no pure LD, HD, and MC phases in CHI for reasons very similar to the reasons for nonexistence of those phases in CHI with an extended defect, as discussed above.

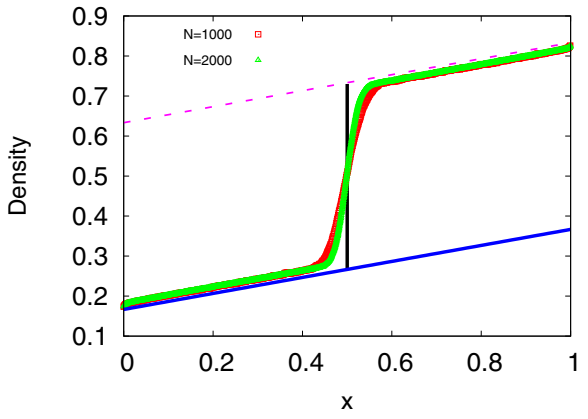

FIG. 6. (Color online) Density plot for $x_L > x_R$. $\Omega = 0.2$, $p = 0.2$. The square points and the triangular points show MCS results for $N = 1000$ and $N = 2000$, respectively. The black line corresponds to the position of DW according to MFT. The gapped and solid lines represent n_R and n_L MFT equations, respectively. It can be seen that the DW becomes sharper on increasing the system size.

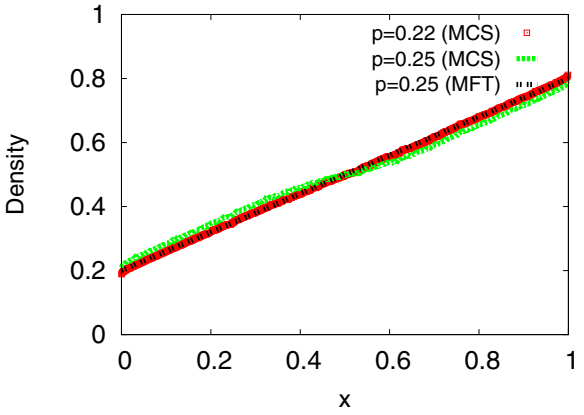

FIG. 7. (Color online) Straight-line profile for the point defect ($x_L = x_R$, $N = 1000$). Even though qualitatively MFT and MCS agree, minor quantitative disagreements between the two for the point defect case can be seen. The dotted black line represents the MFT density-profile equation for $\Omega = 0.6$, $p = 0.25$ and the green line shows the corresponding MCS result. The red points correspond to the MCS density profile for $\Omega = 0.6$, $p = 0.22$.

C. Phase diagram for a point defect

To construct the phase diagram in the Ω-p plane, we identify the threshold line for crossover from three-phase to two-phase coexistence. The crossover line is obtained by the condition $x_L = x_R$. This yields

$$p = \frac{1-\Omega}{1+\Omega}. \tag{27}$$

The phase boundary is shown in Fig. 9. Following our analysis above for an extended defect, we consider the width of the MC phase, $W_p = x_R - x_L > 0$, as the order parameter for the phase transition between the three- and two-phase coexistences; W_p is zero in the two-phase coexistence. Again

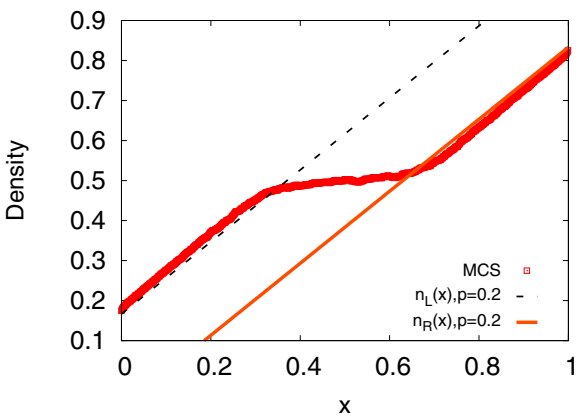

FIG. 8. (Color online) Density plot for three-phase coexistence for the point defect. $\Omega = 0.9$, $p = 0.2$, $N = 1000$. The gapped and solid lines represent MFT equations while the square points are obtained from MCS.

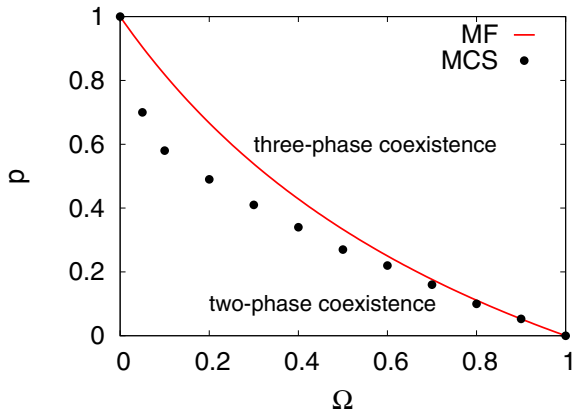

FIG. 9. (Color online) The phase diagram for a point defect. The curve $p = (1 - \Omega)/(1 + \Omega)$ separates regions of two-phase and three-phase coexistences.

as above, W_p depends linearly on δp_p and $\delta\Omega_p$, where $p = p_{cp} + \delta p_p$, $\Omega = \Omega_{cp} - \delta\Omega_p$; Ω_{cp} and p_{cp} satisfy Eq. (27). Clearly, W_p vanishes smoothly as δp_p and $\delta\Omega_p$, indicating the second-order nature of the phase transition. Again, the corresponding order parameter exponent is unity, same as that for an extended defect.

IV. COMPARISON BETWEEN THE DENSITY PROFILES WITH EXTENDED AND POINT DEFECTS

We find that with both extended and point defects, the system can be either in three-phase or two-phase coexistence. As a result, the phase diagram Eqs. (5) and (9), respectively, for extended and point defects have similar structures. However, the precise phase boundaries in the two cases differ significantly quantitatively. Similar differences are observed in plots of density profiles with both extended and point defects; for plots of density versus x, see Figs. 10 and 11 for point defects and Fig. 12 for extended defect. The difference

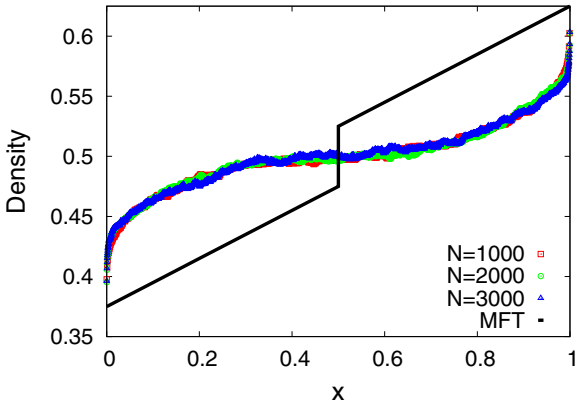

FIG. 11. (Color online) Mismatch between MFT and MCS predictions for the density profile with a point defect [$\Omega = 0.2$, $p = 0.6$, $N = 1000$ (square), 2000 (circle), 3000 (triangle)]. While the MFT solutions, shown by the continuous black lines (with LDW at $x = 0.5$) for the given values of Ω and p display a two-phase coexistence, MCS data points for all the three values of N display a three-phase coexistence. This disagreement is also visible in Fig. 9, where the MCS and MFT phase boundaries differ substantially for small Ω.

between MFT and MCS results is markedly visible in Fig. 11, i.e., for sufficiently small Ω. Figure 9 shows that for a certain range of values of the phase parameters p and Ω, MFT and MCS yield contrasting results. For example, density profiles for a point defect ($p = 0.6, \Omega = 0.2$) are shown in Fig. 11. These chosen values of p and Ω are such that they lie in the region of the phase space where MFT and MCS phase boundaries do not overlap (see Fig. 9). These disagreements are clearly visible in Fig. 11. While the thick continuous lines (with LDW at $x = 0.5$) in Fig. 11 correspond to MFT solutions for the two-phase coexistence with $p = 0.6$, $\Omega = 0.2$ [see Eqs. (22)], the MCS studies, on the other hand, show three-phase coexistence for the same p and Ω (data points in Fig. 11). The MCS results for $N = 1000, 2000, 3000$ show

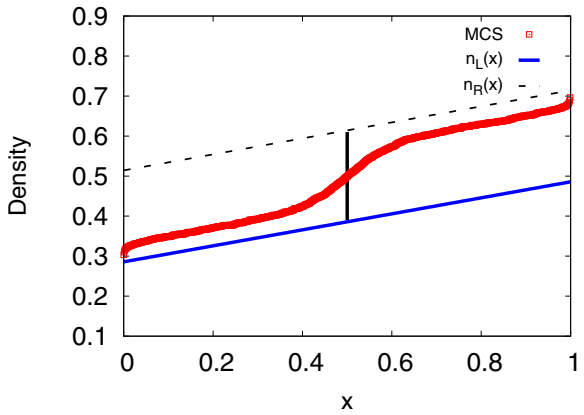

FIG. 10. (Color online) Plot of the density profile for a point defect displaying the mismatch between MFT and MCS predictions ($\Omega = 0.2$, $p = 0.4$, $N = 1000$). The black line at $x = 0.5$ corresponds to the MFT LDW. Gapped and solid straight lines refer to MF equations for $n_R(x)$ and $n_L(x)$, respectively. Square points show MCS results.

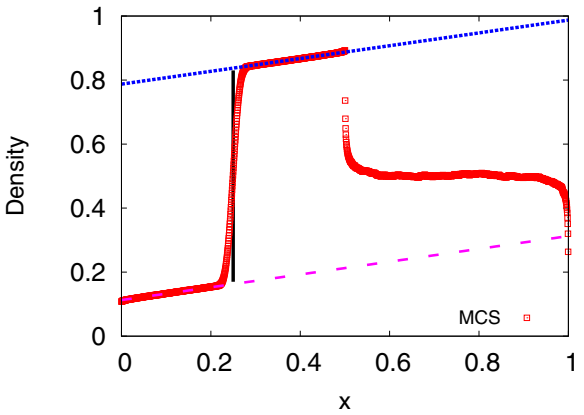

FIG. 12. (Color online) Density profile for the system with an extended defect ($\Omega = 0.2$, $p = 0.4$, $N = 2000$) showing strong agreement between MCS and MFT predictions. The black vertical line corresponds to the MFT LDW. Thin gapped [$n_{1\alpha}(x)$] and thick broken [$n_{1\beta}(x)$] lines refer to the MF equations. The square points show the MCS results.

no systematic system size dependencies and overlap with each other. Notice that the relative quantitative inaccuracies of MFT in a closed ring TASEP with a point defect without any LK, in comparison with a closed TASEP with extended defects (again without LK), have been known; see, e.g., Refs. [10] and [11] for studies on closed TASEPS with point and extended defects, respectively. It is, perhaps, not a surprise that for small Ω, some of theses mismatches are observed in our model as well.

These differences may be understood in terms of the differences in the steady-state currents across the defects in the two cases. In case of an extended defect, the current in the neighborhood of the junctions A and B is $J_e = p/4$, where as it is $J_p = p/(1+p)^2$ very close to a point defect. Thus, $J_e < J_p$ generically, since $p < 1$. Now, the existence of a three-phase coexistence requires the currents rising from low values (J_e or J_p, as the case may be) to 1/4. The corresponding densities in CHI also vary *linearly* with slope Ω from low or high values near the extended or point defects to reach $1/2$ at the meeting points with the MC part of the three-phase coexistence, i.e., at x_α and x_β for an extended defect and x_L and x_R for a point defect. Since $J_e < J_p$ generically, the corresponding values of $n_I(x)$ near a point defect is *closer* to $1/2$ than they are near the junctions A and B with an extended defect: $n_{I\alpha}(x=0) < n_L(x=0)$ and $n_{I\beta}(x=l) > n_R(x=1)$ for a given p. Now, for a given Ω, the slope of the spatially varying solutions for $n_I(x)$ are same (Ω) for both extended and point defects. The densities $n_{I\alpha}(x)$, $n_{I\beta}(x)$ (for an extended defect) and $n_L(x)$, $n_R(x)$ (for a point defect) must reach $1/2$ in the bulk for the MC phase to exist. Hence, with an extended defect for a given p higher values of Ω are required for the system to reach the threshold of existence for the MC part of the three-phase coexistence. This explains the quantitative differences in the phase boundaries in the phase diagram Eqs. (5) and (9).

Notice that for the phase boundary corresponding to an extended defect (Fig. 5), the level of quantitative agreement between the MFT and MCS results for small-Ω is much stronger than in the phase diagram (Fig. 9) for a point defect. Similarly, density profiles for a point defect show much larger discrepancy between the MCS and the MFT results, in comparison with the same for an extended defect; see Figs. 10 and 11 for a point defect, which clearly display the quantitative disagreement between MCS and MFT results. In fact, this disagreement is revealed vividly in Fig. 11, where the density profile obtained from MCS describes a three-phase coexistence, where as MFT predicts a two-phase coexistence. In contrast, the density profile for CHI with an extended defect as obtained from MCS match very well with the corresponding MFT prediction; see Fig. 12. These features may be qualitatively understood as follows. In the small-Ω limit, the effects of particle nonconservation is small, particle number is weakly conserved, and hence the correlation effects due to (weak) conservation of particle number should be substantial, rendering MFT quantitatively inaccurate. For an extended defect with $0 < l < 1$, the total particle number in CHI should fluctuate within a range $l/2 \pm (1-l)/2$, assuming $l > 1-l$ and the averaging occupation number to be $1/2$ in CHI and CHII (borne out by our MCS and MFT). Thus, even in the small-Ω limit, particle number fluctuations in CHI is expected to be still substantial with an extended defect, weakening the correlation effects. This explains the good agreement between the MFT and MCS for extended defects. In contrast, for a point defect the total particle number fluctuations in CHI should vanish in the small-Ω limit, since $l \to 1$ or CHII has a vanishingly small size. Hence, the correlation effects should be large, causing larger discrepancies between the MCS and MFT results for a point defect in the small-Ω limit. For larger Ω, LK ensures lack of any correlation effect regardless of a point or an extended defect, leading to good agreements between MFT and MCS results for both of them.

V. WHY $n = 1/2$ FOR ALL p AND Ω?

As we have shown above, for both point and extended defects, the system is half-filled in the steady state, i.e., the global average density $n = 1/2$ for all Ω and p, disregarding the possible boundary layers (which have vanishing thickness in the thermodynamic limit). This result may be easily obtained by using the MF form of $n_I(x)$ [and also of $n_{II}(x)$ in case of an extended defect] as given above for point and extended defects; our MCS results also validate this to a good accuracy. That $n = 1/2$ generically in our model may be understood physically as follows. Notice that if we set $p = 1$ (homogeneous limit), the model is translationally invariant and the average steady-state density *at every site* is $1/2$. Thus, there are equal number of particles and holes on average. A shift of n from $1/2$ would indicate either more particles or more holes in the system in the steady state. However, even when inhomogeneity is introduced ($p < 1$), there is nothing that favors either particles or holes, since the inhomogeneity that acts as an inhibitor for the particle current also acts as an inhibitor for the holes equally. Thus, it is expected to have equal number of particles and holes on average, i.e., $n = 1/2$ even with $p < 1$. Notice that this argument does not preclude any local excess of particles or holes, since the particles and the holes move in the opposite directions, and hence the presence of a defect should lead to excess particles on one side and excess holes (equivalently deficit particles) on the other side of it. This holds for any Ω, including $\Omega \to 0$, and rules out a pure LD or a pure HD phase. This is in contrast with coupled TASEP and LK with open boundaries [6], where the boundary conditions explicitly favor more particles or holes, and consequently make pure LD or HD phases possible; in the limit of small-Ω, the boundary conditions dominate and the density profiles smoothly crossover to those of pure open TASEP. In contrast, in the present model, the density profiles do not smoothly crossover to those for a closed TASEP (with uniform density) for any small-Ω. Instead, however, for $\Omega \to 0$, the LDW height Eqs. (12) and (26), respectively, for extended and point defects with LK smoothly reduce to the results of Refs. [9] and [13], respectively, with $n = 1/2$.

VI. SUMMARY AND OUTLOOK

In this article, we have constructed an asymmetric exclusion process on an inhomogeneous ring with LK. Our MFT and MCS results reveal that in the limit when TASEP along the ring competes with LK, the model displays inhomogeneous steady-state density profiles and phase transitions between different states of coexistence, parametrized by the scaled LK

rate Ω and hopping rate $p < 1$ at the defect site(s). The model always has a mean density $n = 1/2$ for all Ω and p; as a result there are no pure LD or HD phases, in contrast to LK-TASEP with open boundaries. Our model may be extended in various ways. For instance, we may consider unequal attachment (ω_A) and detachment ω_D rates ($\omega_A/\omega_D = K \neq 1$). In this case, by using the arguments above, $n = K/(1+K)$, see Ref. [6], and can be more or less than $1/2$. Thus, far more complex phase behavior, including spatially varying LD or HD phases, should follow [6]. Details will be discussed elsewhere. Additionally, one may introduce multiple defect segments or point defects. However, unlike Refs. [10,11], no delocalized domain walls (DDW) are expected even when various defect segments or point defects have same hopping rates. This is because DDWs in Refs. [10,11] are essentially consequences of the strict particle number conservations in the models there, the latter being absent in the presence of LK. Our results very amply emphasize the relevance of the ring or closed geometry of the system in the presence of LK. The simplicity of our model limits direct applications of our results to practical or experimental situations. Nonetheless, our results in the context of traffic along a circular track with constrictions or ribosome translocations along mRNA loops with defects, together with random attachments or detachments, generally show that the steady-state densities should be *generically inhomogeneous* regardless of the details of the defects. We hope experiments on ribosomes using ribosome profiling techniques [15] and numerical simulations of more detailed traffic models should qualitatively validate our results.

A few technical comments are in order. First of all, notice that our MFT analysis is equivalent to considering CHI as an open TASEP with self-consistently obtained injection (α_e/α_p) and extraction (β_e/β_p) rates, with $\alpha_e = \beta_e \leqslant 1/2$ and $\alpha_p = \beta_p \leqslant 1/2$, as obtained above. Given this analogy with an open TASEP, we can now compare our results with that of Ref. [6], which has investigated an open TASEP with LK. With the conditions on $\alpha_{e,p}$ and $\beta_{e,p}$, our results should correspond to the $\alpha = \beta \leqslant 1/2$ line in the phase diagrams of Ref. [6], where α and β are the injection and extraction rates in Ref. [6]. Now notice that in Ref. [6] along the line $\alpha = \beta \leqslant 1/2$ only two-phase and three-phase coexistences are possible, in agreement with our results here. Furthermore, as in Ref. [6], two-phase coexistence is found for small α, β, which in our model means small p, where as for large p, three-phase coexistence is found. Our MFT is based on analyzing the bulk density profile, neglecting the boundary layers. An alternative powerful theoretical approach to TASEP-like models with open boundaries have been formulated that makes use of the boundary layer itself, instead of the bulk [16]. It will be interesting to extend these ideas to TASEP on a closed ring with LK.

ACKNOWLEDGMENTS

One of the authors (A.B.) gratefully acknowledges partial financial support by the Max-Planck-Gesellschaft (Germany) and Indo-German Science & Technology Centre (India) through the Partner Group programme (2009). A.K.C. acknowledges the financial support from Council of Scientific and Industrial Research (CSIR) under the Senior Research Associateship [Grant No. 13(8745-A)/2015-Pool].

[1] I. Kosztin and K. Schulten, Phys. Rev. Lett. **93**, 238102 (2004).
[2] J. MacDonald, J. Gibbs, and A. Pipkin, Biopolymers **6**, 1 (1968); R. Lipowsky, S. Klumpp, and T. M. Nieuwenhuizen, Phys. Rev. Lett. **87**, 108101 (2001).
[3] J. Kärger and D. Ruthven, *Diffusion in Zeolites and Other Microporous Solids* (Wiley, New York, 1992).
[4] B. Alberts *et al.*, *Molecular Biology of the Cell* (Garland Science, New York, 2002).
[5] D. Chowdhury, L. Santen, and A. Schadschneider, Phys. Rep. **329**, 199 (2000); D. Helbing, Rev. Mod. Phys. **73**, 1067 (2001); T. Chou, K. Mallick, and R. K. P. Zia, Rep. Prog. Phys. **74**, 116601 (2011).
[6] A. Parmeggiani, T. Franosch, and E. Frey, Phys. Rev. E **70**, 046101 (2004).
[7] J. J. Dong, B. Schmittmann, and R. K. P. Zia, J. Stat. Phys. **128**, 21 (2007); P. Greulich and A. Schadschneider, Physica A **387**, 1972 (2008); R. K. P. Zia, J. J. Dong, and B. Schmittmann, J. Stat. Phys. **144**, 405 (2011); J. S. Nossan, J. Phys. A: Math. Theor. **46**, 315001 (2013).
[8] P. Pierobon, M. Mobilia, R. Kouyos, and E. Frey, Phys. Rev. E **74**, 031906 (2006).
[9] G. Tripathy and M. Barma, Phys. Rev. E **58**, 1911 (1998).
[10] N. Sarkar and A. Basu, Phys. Rev. E **90**, 022109 (2014).
[11] T. Banerjee, N. Sarkar, and A. Basu, J. Stat. Mech.: Theory Exp. (2015) P01024.
[12] T. Chou, Biophys. J. **85**, 755 (2003); S. E. Wells, E. Hillner, R. D. Vale, and A. B. Sachs, Mol. Cell. **2**, 135 (1998); S. Wang, K. S. Browning, and W. A. Miller, EMBO J. **16**, 4107 (1997); G. S. Kopeina *et al.*, Nucleic Acids Res. **36**, 2476 (2008).
[13] S. A. Janowsky and J. L. Lebowitz, Phys. Rev. A **45**, 618 (1992).
[14] P. M. Chaikin and T. C. Lubensky, *Principles of Condensed Matter Physics* (Cambridge University Press, Cambridge, 2000).
[15] Y. Arava *et al.*, Nucl. Acids Res. **33**, 2421 (2005); N. T. Ingolia *et al.*, Science **324**, 218 (2009); H. Guo *et al.*, Nature **466**, 835 (2010).
[16] S. Mukerjee and S. M. Bhattacharjee, J. Phys. A: Math. Gen. **38**, L285 (2005); S. Mukherji and V. Mishra, Phys. Rev. E **74**, 011116 (2006); S. M. Bhattacharjee, J. Phys. A: Math. Theor. **40**, 1703 (2007); S. Mukherji, Phys. Rev. E **79**, 041140 (2009); **83**, 031129 (2011); A. K. Gupta and I. Dhiman, *ibid.* **89**, 022131 (2014).